minerals

MDPI

Article

Wardite ($NaAl_3(PO_4)_2(OH)_4 \cdot 2H_2O$) at High Pressure: Compressional Behavior and Structure Evolution

G. Diego Gatta [1,*], Davide Comboni [2], Paolo Lotti [1], Alessandro Guastoni [3], Nicola Rotiroti [1] and Michael Hanfland [2]

[1] Dipartimento di Scienze della Terra, Università degli Studi di Milano, Via Botticelli 23, I-20133 Milano, Italy; paolo.lotti@unimi.it (P.L.); nicola.rotiroti@unimi.it (N.R.)
[2] European Synchrotron Radiation Facility—ESRF, 71 Avenue des Martyrs, F-38000 Grenoble, France; davide.comboni@esrf.fr (D.C.); hanfland@esrf.fr (M.H.)
[3] Dipartmento di Geoscienze, Università degli Studi di Padova, Via G. Gradenigo 6, I-35131 Padova, Italy; alessandro.guastoni@unipd.it
* Correspondence: diego.gatta@unimi.it; Tel.: +39-02-503-15607

Received: 9 September 2020; Accepted: 29 September 2020; Published: 1 October 2020

Abstract: The high-pressure behavior of wardite, $NaAl_3(PO_4)_2(OH)_4 \cdot 2H_2O$ (a = 7.0673(2) Å, c = 19.193(9) Å, Sp. Gr. $P4_12_12$), has been investigated by in-situ single-crystal synchrotron diffraction experiments up to 9 GPa, using a diamond anvil cell under quasi-hydrostatic conditions. This phosphate does not experience any pressure-induced phase transition, or anomalous compressional behavior, within the pressure-range investigated: its compressional behavior is fully elastic and all the deformation mechanisms, at the atomic scale, are reversible upon decompression. A second-order Birch–Murnaghan Equation of State was fitted to the experimental data, weighted by their uncertainty in pressure (P) and volume (V), with the following refined parameters: V_0 = 957.8(2) Å^3 and $K_{V0} = -V_0(\partial P/\partial V)_{P0,T0}$ = 85.8(4) GPa ($\beta_{V0} = 1/K_{V0}$ = 0.01166(5) GPa^{-1}). Axial bulk moduli were also calculated, with: $K_0(a)$ = 98(3) GPa ($\beta_{0(a)}$ = 0.0034(1) GPa^{-1}) and $K_0(c)$ = 64(1) GPa ($\beta_{0(c)}$ = 0.0052(1) GPa^{-1}). The anisotropic compressional scheme is: $K_0(a)$:$K_0(c)$ = 1.53:1. A series of structure refinements were performed on the basis of the intensity data collected in compression and decompression. The mechanisms at the atomic scale, responsible for the structure anisotropy of wardite, are discussed.

Keywords: wardite; phosphates; synchrotron single-crystal diffraction; high-pressure; compressibility

1. Introduction

Wardite, ideally $NaAl_3(PO_4)_2(OH)_4 \cdot 2H_2O$, is a hydrous phosphate discovered at the end of the nineteenth century [1,2]. It is a hydrothermal mineral, which usually occurs in *P*-rich zones of granite pegmatites and also in sedimentary iron-rich formations. Its crystal structure (as H-free model) was solved by Fanfani et al. [3], on the basis of single-crystal X-ray intensity data (collected by the Weissenberg method) and recently reinvestigated by Gatta et al. [4] by means of single-crystal neutron diffraction (at 20 K). Gatta et al. [4] provided a full location of all the H sites, along with the description of their anisotropic displacement regime and the complex H-bonding network (wardite contains up to 18 wt% of H_2O). Wardite's structure is tetragonal, space group $P4_12_12$, with $a = b \sim 7.06$ Å and $c \sim 19.1$ Å. X-ray and neutron structure refinements confirmed that the structure of this mineral consists of sheets made by edge-sharing Na-polyhedra (CN = 8) and Al-octahedra along with vertex-sharing Al-octahedra, parallel to (001) and connected by P-tetrahedra and H-bonds to form a (001) layer-type structure (Figure 1). This topology explains the pronounced {001} cleavage commonly observed in wardite crystals, shared with the fluorowardite variant (ideally $NaAl_3(PO_4)_2(OH)_2F_2 \cdot 2H_2O$, [2]).

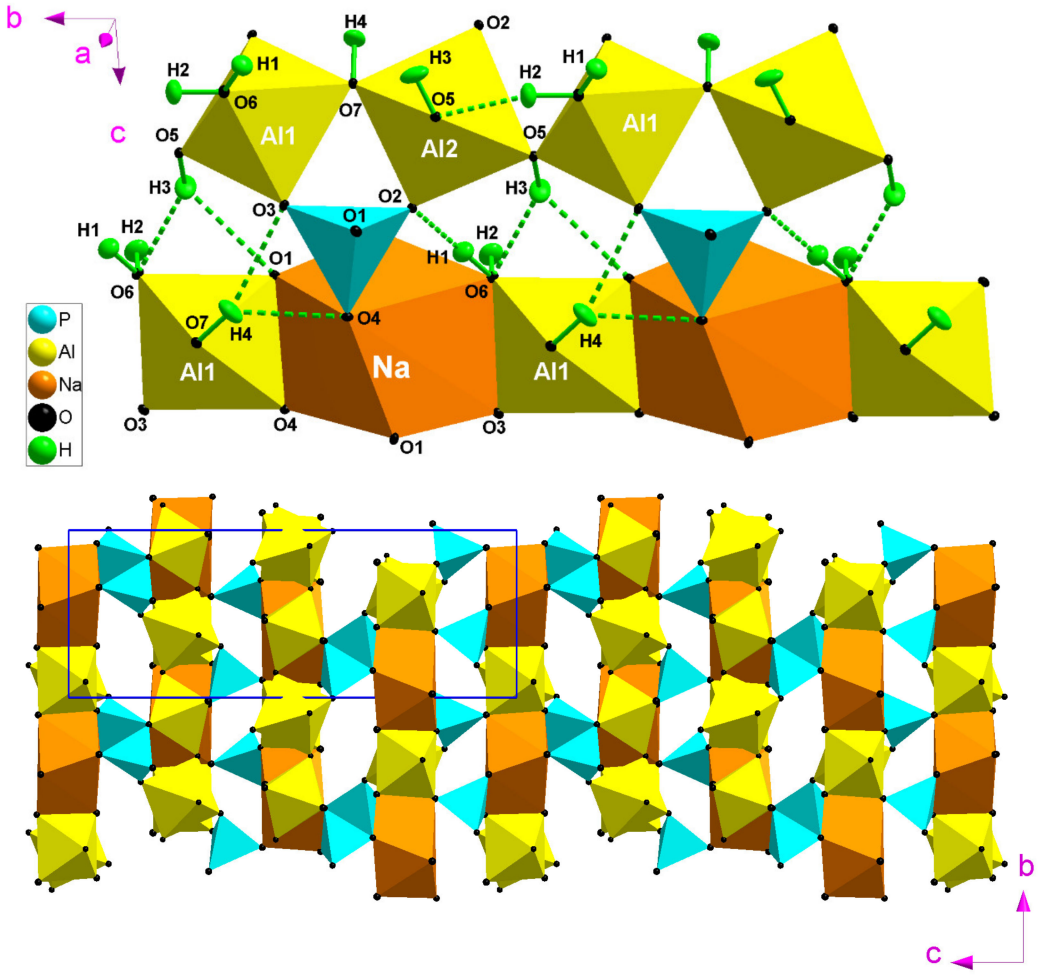

Figure 1. (**Bottom**) A view of the crystal structure of wardite down {100} (the unit-cell in blue). (**Top**) Details of the crystal structure and H-bonding network (based on the neutron structure refinement by Gatta et al. [4]).

The structure of wardite contains hydroxyl groups and H_2O molecules. Gatta et al. [4] reported that whereas the unique H_2O molecule (i.e., H1-O6-H2) experiences two strong H-bonds, as corroborated by the bonding geometry (i.e., O6-H1 ... O2 = 174.4(1)° and H1 ... O2 = 1.617(1) Å, O6-H2 ... O5 = 160.1(1)° and H2 ... O5 = 1.913(1) Å), the two independent hydroxyl groups (i.e., O5-H3, O7-H4) show relatively weak interactions with bifurcated bonding configurations (i.e., O5-H3 ... O1 = 139.9(1)° and H3 ... O1 = 2.556(1) Å, and O5-H3 ... O6 = 148.5(1)° and H3 ... O6 = 2.347(1) Å; O7-H4 ... O3 = 160.5(1)° and H4 ... O3 = 2.447(1) Å, O7-H4 ... O4 = 137.9(1)° and H4 ... O4 = 2.449(1) Å) (Figure 1). The hydrogen bonds of the H_2O molecule show O-H ... O angles ≥ 170°, with a configuration energetically favorable (i.e., toward linearity); the bifurcated H-bonding configurations of the two independent hydroxyl groups leads to a bonding geometry energetically unfavorable. As a matter of fact, in fluorowardite (ideally $NaAl_3(PO_4)_2(OH)_2F_2{\cdot}2H_2O$), one of the two independent hydroxyl groups is replaced by fluorine, but the H_2O content and configuration are virtually identical to that of wardite: the replacement $OH^- \rightarrow F^-$ does not generate any significant rearrangement of the structure because of the weak H-bonds of the hydroxyl groups. The H-bonding network reported by Gatta et al. [4] for wardite is compatible with the previous experimental findings based on vibrational spectroscopies (e.g., [5–7]).

Some open questions concerning this phosphate are: How does wardite behave at high pressure? Does it experience any pressure-induced phase transition? Which is the role played by the complex H-bonding network on its compressional pattern? The behavior of wardite at high pressure is completely unexplored. It is unknown its compressional pattern (soft or stiff? how anisotropic?),

its high-*P* phase stability field and the mechanisms, at the atomic scale, which allow the structure to accommodate the effects of the applied pressure. In this light, the aim of this study is to investigate the high-pressure behavior of wardite by means of in-situ single-crystal X-ray diffraction using a diamond anvil cell (DAC), under quasi-hydrostatic conditions. This study represents the first step of a larger project on this class of materials, and the thermodynamic parameters here obtained will serve for any potential modeling of the phase-stability and behavior under non-ambient conditions of this hydrous phosphate, with geological or industrial implications.

2. Materials and Methods

The sample of wardite used in this study belongs to the collection of the Museum of Mineralogy of the University of Padova (catalogue number MM18662), and it is the same already used for the neutron diffraction experiment recently performed by Gatta et al. [4]. The hand specimen is made by large and transparent crystals, collected at the Rapid Creek area, Canada. A geological description of the Rapid Creek area was reported by Robertson [8], with deposits of siderite and phosphatic ironstone embedded in shales and sequences of sandstones, the early to mid-Cretaceous "Blow River Formation". The phosphatic iron formation contains phosphate-siderite grains, quartz and skeletal fragments in a matrix of sideritic mudstone. Most of the phosphate grains are composed by rare phosphate minerals (e.g., arrojadite, gormanite and satterlyite). Well-crystallized phosphates occur within fractures that cross-cut the Blow River Formation, in which the wardite sample (used in this study) is associated with gormanite and siderite. No geological evidence of igneous activity, in the area, was found. Fluid inclusion studies reported that the sequence of crystallization of phosphates at Rapid Creek occurred between 180 and 200 °C, with quartz, lazulite and arrojadite representing the first minerals to crystallize, whereas wardite was a late stage phosphate. According to Robinson et al. [9], the fracture-filling minerals were probably formed in the uppermost diagenesis to the lowermost range of regional metamorphism.

Wardite is one of the phosphates used as gemstone, because of its occurrence as centimetric and pale colored crystals (lightly colored blue to green, yellow-green, light yellow, brown). Its hardness (5 on Mohs scale) represents the main limitation for its utilization in jewelry. It is cut more frequently as cabochons than as faceted stone. To the best of our knowledge, wardite crystals used as gemstones are those from the Rapid Creek area, Canada. Crystals from other localities, e.g., Brazil (Paraíba, Alto Patrimônio) and USA (Maine, Dunton Gem Quarry; Utah, Little Green Monster Variscite Mine) are not gem-quality and used for collections.

As described by Gatta et al. [4], the chemical composition of the crystal of wardite used for this study was obtained by EPMA-WDS, giving the following empirical formula: $(Na_{0.91}Ca_{0.01})_{\Sigma=0.92}(Al_{2.97}Fe^{3+}_{0.05}Ti_{0.01})_{\Sigma=3.03}(P_{2.10}O_8)(OH)_4 \cdot 1.74H_2O$. However, the neutron structure refinement provided evidence of an ideal H_2O content, with 2.0 molecules per formula unit [4]. The authors ascribed the small deficit of H_2O based on the EPMA-WDS data to a partial dehydration under the electron beam [4] (operating conditions: 20 kV accelerating voltage, 5 nA beam current and 10 μm beam diameter, counting times of 10 s at the peak and 5 s at the background for major elements, and 20–100 s at peak and background for minor elements).

A crystal with size ~50 × 40 × 20 μm^3 was selected for the X-ray diffraction experiment. In-situ high-pressure single-crystal X-ray diffraction experiment was performed at the synchrotron beamline ID15-b, at the ESRF, Grenoble (France). A stainless-steel foil (with thickness ~250 μm) was pre-indented to 70 μm and then drilled by spark-erosion, leading to a *P*-chamber of ~300 μm in diameter. The crystal was loaded in the pressure-chamber of a membrane-driven DAC, with 600-μm culet Boehler-Almax design anvils. Ruby spheres were used as *P*-calibrant (pressure uncertainty ±0.05 GPa, [10]) and the methanol:ethanol:H_2O = 16:3:1 mixture was used as quasi-hydrostatic *P*-transmitting fluid [11]. A convergent monochromatic beam (E ~ 30 keV, λ ~ 0.4101 Å) was used for the X-ray diffraction experiment. The diffraction patterns were collected by a MAR555 flat-panel detector, positioned at about 280 mm from the sample position. Sample-to-detector distance was calibrated using a Si powder standard and an enstatite ($MgSiO_3$) crystal. Further details on the beamline setup are reported in Merlini

and Hanfland [12]. The data collection strategy consisted in a pure ω-scan (−32° ≤ ω ≤ +32°), with 0.5° step width and 0.5 s exposure time per step. High-*P* data were collected up to ~9 GPa, and to assess the reversibility of the compressional pattern, a few data-points were collected also in decompression (19 data-points in compression, 3 in decompression). The CrysAlis package [13] was used to index the diffraction peaks and to integrate their intensities (corrected for Lorentz-polarization effects). Correction for absorption (caused by the DAC components) was applied using the semi-empirical *ABSPACK* routine, implemented in CrysAlis [13].

Structure refinements were performed using the software Jana 2006 [14], starting from the (H-free) model reported by Gatta et al. [4]. All the crystallographic sites were modeled as fully occupied, using the neutral scattering curves of Na, Al, P and O. Due to the reciprocal lattice coverage limitations, induced by the DAC components, the atomic displacement parameters were all modeled as isotropic. All the refinements converged with no significant correlations among the refined variables, as shown by the variance–covariance matrix, and insignificant residuals in the difference-Fourier maps of the electron density function. The relevant statistical parameters pertaining to the structure refinements are listed in Table S1 (deposited). The atomic coordinates, along with the isotropic displacement parameters, and the relevant polyhedral bond distances are reported in Table S2 (deposited). Polyhedral volumes with pressure are listed in Table S3 (deposited). The results of all the structure refinements are also deposited as Crystallographic Information Files (CIF).

3. Results

3.1. Compressional Behavior

The evolution of the unit-cell parameters of wardite with pressure is reported in Table 1 and shown in Figure 2. No phase transition, or anomalous compressional behavior, has been observed within the pressure-range investigated. Although only a few data points were collected in decompression, they confirm a full elastic behavior of the mineral up to the maximum pressure achieved in this experiment. In decompression, the slight deviations observed for the lengths of the unit-cell edges, with respect to the compressional trends, are mutually compensated for the unit-cell volume (Figure 2).

Table 1. Unit-cell parameters of wardite with pressure (* data collected in decompression).

P (GPa)	*V* (Å^3)	*a* (Å)	*c* (Å)
0.0001	958.6(5)	7.0673(2)	19.193(9)
0.15(5)	956.9(4)	7.0677(2)	19.156(8)
0.32(5)	954.5(4)	7.0634(2)	19.132(8)
0.53(5)	951.4(4)	7.0568(2)	19.104(8)
0.85(5)	948.2(5)	7.0505(2)	19.075(8)
1.18(5)	943.8(4)	7.0390(2)	19.048(8)
1.55(5)	940.7(4)	7.0349(8)	19.008(8)
2.12(5)	934.8(4)	7.0203(2)	18.968(8)
2.63(5)	930.9(4)	7.0128(2)	18.929(8)
3.27(5)	924.5(4)	6.9976(2)	18.880(7)
3.88(5)	918.4(4)	6.9846(2)	18.826(8)
4.70(5)	911.1(4)	6.9691(2)	18.760(8)
5.45(5)	904.5(4)	6.9559(2)	18.694(8)
6.55(5)	896.1(4)	6.9377(2)	18.617(8)
6.99(5)	892.6(4)	6.9288(2)	18.592(8)
7.68(5)	886.4(4)	6.9155(2)	18.535(7)
8.08(5)	884.0(4)	6.9120(2)	18.502(9)
8.78(5)	879.3(3)	6.9016(2)	18.461(7)
9.08(5)	876.7(3)	6.8935(1)	18.449(7)
6.95(5) *	893.6(3)	6.9309(1)	18.602(7)
1.78(5) *	939.4(1)	7.0387(4)	18.961(8)
0.0001 *	958.3(8)	7.0805(2)	19.115(10)

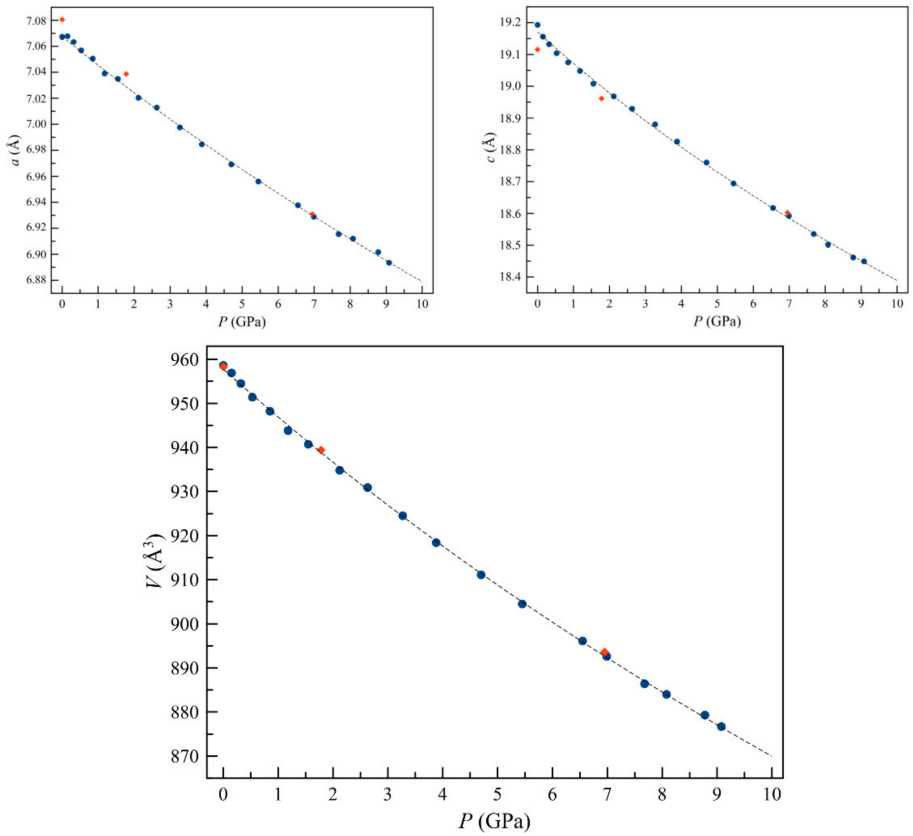

Figure 2. Evolution of the unit-cell parameters of wardite with *P*. Red diamonds: data collected in decompression. Dashed lines represent the Equation of State (EoS) fits (see text for details). Error bars are smaller than symbols.

The compressional behavior of wardite was modeled with the isothermal Birch–Murnaghan Equation of State (BM-EoS) [15], which is based on the assumption that the high-pressure strain energy in a solid can be expressed as a Taylor series in the Eulerian finite strain, defined as $fe = [(V_0/V_P)^{2/3} - 1]/2$. For wardite, the evolution of the Eulerian finite strain vs. the normalized pressure (*Fe*, defined as $Fe = P/3fe(1 + 2fe)^{5/2}$), calculated using the Eos_Fit7c software [16], shows an almost horizontal trend (Figure 3), confirming that a truncation to the second-order (in energy) Birch–Murnaghan EoS provides the best figure of merit. Fitting the experimental data, weighted by their uncertainty in *P* and *V*, with an EoS truncated to the second-order, yielded to the following refined parameters: $V_0 = 957.8(2)$ Å^3, $K_{V0} = -V_0(\partial P/\partial V)_{P0,T0} = 85.8(4)$ GPa ($\beta_{V0} = 1/K_{V0} = 0.01166(5)$ GPa^{-1}) (Table 2). Elastic parameters using a third-order BM-EoS have also been calculated, and listed in Table 2.

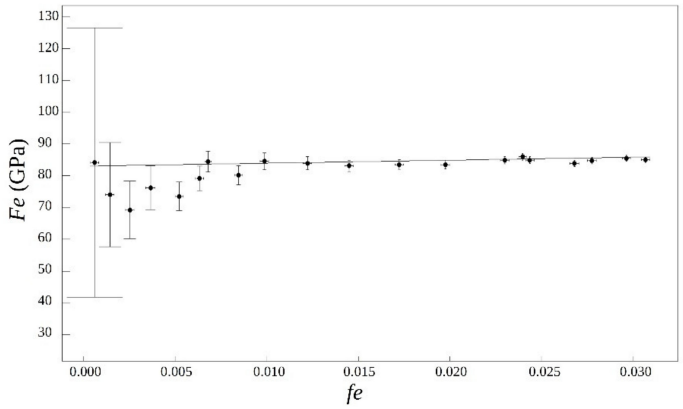

Figure 3. *fe-Fe* plot based on the data of wardite collected between 0.0001 and 9.08 GPa.

Table 2. Refined elastic parameters of wardite, based on the isothermal II- and III-Birch–Murnaghan (BM) Equation of State fits (* fixed parameter).

Unit-Cell Parameters	V_0, x_0 (Å^3, Å)	$K_{V0,\,x0}$ (GPa)	K'	$\beta_{V0,\,x0}$ (GPa^{-1})
V	957.8(2)	85.8(4)	4 *	0.01166(5)
a	7.074(1)	98(3)	4 *	0.0034(1)
c	19.161(7)	64(1)	4 *	0.0052(1)
II-BM EoS, 0.0001 < P < 9.08(5) GPa				
V	958.2(2)	82(2)	4.9(5)	0.0122(3)
a	7.0675(4)	102(2)	5(1)	0.0033(1)
c	19.17(1)	63(5)	4(1)	0.0053(5)
III-BM EoS, 0.0001 < P < 9.08(5) GPa				

Axial bulk moduli were calculated with a second-order "linearized" BM-EoS [17]. The refined linear-EoS parameters for wardite are: a_0 = 7.074(1) Å and $K_0(a)$ = 98(3) GPa ($\beta_{0(a)}$ = 0.0034(1) GPa^{-1}) for the *a*-axis; c_0 = 19.161(7) Å and $K_0(c)$ = 64(1) GPa ($\beta_{0(c)}$ = 0.0052(1) GPa^{-1}) for the *c*-axis. The anisotropic compressional scheme is: $K_0(a)$:$K_0(c)$ = 1.53:1 (Table 2).

3.2. Results: Structure Evolution at High Pressure

The evolution with *P* of bond distances and angles of the (H-free) structure model of wardite can be deduced on the basis of the data reported in Tables S2—S4 (deposited) and in the CIFs (deposited). Variations in response to the applied pressure are continuous and monotonic. Here we provide, in particular, an analysis of the deformation mechanisms, at the atomic scale, which can generate the compressional anisotropy described in the previous section (with $K_0(a)$:$K_0(c)$ = 1.53:1). In the following, we compare the structural data between 0.0001 and 8.08 GPa, avoiding the consideration of data at the highest pressure (≥ 8.8 GPa) approaching the hydrostatic limit of the *P*-transmitting fluid.

It is worthy of note that the P-tetrahedron does not behave as a rigid unit within the *P*-range investigated. Considering the structural data at 0.0001 and 8.08 GPa, we can observe that the contraction of the four independent bond lengths is strongly anisotropic, being Δ(P-O1) = −0.036 Å, Δ(P-O2) = −0.015 Å, Δ(P-O3) = −0.003 Å, and Δ(P-O4) = −0.030 Å (Table S2). The average P-O distance contracts by ca. 0.020 Å. The evolution of the polyhedral volume with pressure of the P-tetrahedron, and its relative compressional parameters, are given in Tables S3 and S4. P-tetrahedra act as bridging units between sheets parallel to (001) made by edge-sharing Na-polyhedra and Al-octahedra along with vertex-sharing Al-octahedra (Figure 1). The role played by the tetrahedral unit on the compressional anisotropy of the whole structure, and in particular along [001], can be deduced by the shortening of the O-O distances of the tetrahedron, and in particular by the compression of the O3-O4, O1-O4 and O2-O4 edges (Figure 1). Their contraction is pronounced within the *P*-range here considered, respectively, by 0.02 Å, 0.08 Å and 0.05 Å. As P-tetrahedra are isolated units on the *ab*-plane, it is reasonable to consider that their role on the compression on (001) is secondary.

On the other hand, even the aforementioned sheets // (001), made by Na-polyhedra and Al-octahedra, are expected to play a role on the structure anisotropy. The contraction of the sheet along [001], in response to the applied pressure, can be represented by the evolution of the distance O3–O6 (edge shared by Na- and Al-polyhedra, Figure 1) and O4-O1 (edge of the Na-polyhedron): the first is substantially unchanged and contracts by only ~0.004 Å, while the second experiences a pronounced compression by ~0.05 Å, for a Δ*P* = 8.08 GPa. The sheets are expected to cause the lower compressibility on (001), as the compression on this plane can be obtained only by contraction of bonds, being other energetically less-costly mechanisms (e.g., polyhedral tilting with resulting sheet corrugation) hindered by the inter-polyhedral bonding configuration (e.g., polyhedral connection by edge-sharing).

The structure refinements at high-*P* do not allow to locate the H sites, hindering a deep analysis of the effect of pressure on the H-bonds (and vice versa). However, if we consider the geometrical

configuration of the H-bonds reported by Gatta et al. [4] (Figure 1), we observe that some bonds have vectors with major components along [001] (e.g., H1 ... O2, H3 ... O6, H3 ... O1, H4 ... O3) and others lying almost on (001) (e.g., H2 ... O5, H4 ... O4). In this light, there must be a given contribution of the H-bonds either along [001] and on (001). Therefore, the H-bonding network likely does not play a relevant role on the compressional anisotropy of the whole structure.

4. Discussion and Conclusions

The compressional experiment on wardite of this study shows that this phosphate does not experience any *P*-induced phase transition, or anomalous compressional behavior, at least up to 9 GPa. In such a *P*-range, its compressional behavior is fully elastic: all the deformation mechanisms at the atomic scale are reversible upon decompression.

The (isothermal) bulk modulus of wardite, derived by a second-order BM-EoS fit to the *P*-*V* data (K_{V0} = 85.8(4) GPa), is significantly high, if compared to other crustal materials. For comparison, the bulk modulus of quartz is ~37 GPa [18], feldspars ~50–60 GPa (e.g., [19] and references therein), micas ~40–60 GPa (e.g., [20,21] and references therein), pyroxenes ~100–120 GPa (e.g., [22] and references therein), and olivines 120–130 GPa (e.g., [23] and reference therein). The bulk modulus of wardite reflects the calculated compressibilities of the building units: the bulk moduli of the P-tetrahedron, Al-octahedra and Na-polyhedron are, respectively, 175(33), 145(25) and 61(5) GPa (Table S4). Surprisingly, the P-tetrahedron is pronouncedly softer than the Si-tetrahedron (e.g., with $K_{V0(SiO4)}$ = 328(42) GPa [24]). It is not clear why the P-tetrahedron is softer than the Si-counterpart, considering the higher bond valence and the shorter bond length of P-O if compared to Si-O. However, the polyhedral compression reflects even the surrounding connections, and it is never independent of the inter-polyhedral bonding configuration.

The isothermal bulk modulus (or its reciprocal parameter: the isothermal compressibility coefficient, $\beta_{V0} = 1/K_{V0}$ = 0.01166(5) GPa^{-1}) here obtained is the first thermodynamic parameter to model the phase stability of this mineral, as single phase or as a component of a rock assemblage. To the best of our knowledge, the bulk thermal expansion coefficient [$\alpha_{V0} = 1/V_0(\partial V/\partial T)_{P0,T0}$], along with the thermal anisotropy of the structure, are still unknown.

The axial compressional anisotropy of wardite is significant ($K_0(a)/K_0(c)$ = 1.53), but not so pronounced as that observed in proper "layered structures", e.g., phyllosilicates in which it can reach even values of $K_0(max)/K_0(min)$ from 3 to 5 ([21,25,26]). As commonly observed in layered structures, even in wardite the softest direction is perpendicular to the sheets, in this case // [001].

The analysis of the structure evolution in response to the applied pressure shows not only that the P-tetrahedron does not behave as a "rigid unit", but even that its deformation is rather anisotropic, with contraction of the bond lengths varying between 0.003 Å and 0.036 Å (for a ΔP = 8.08 GPa). The anisotropic contraction of the P-tetrahedron does not lead to a geometric "regularization" of the polyhedron: the difference between the longest and shortest P-O bond length is ~0.03 Å at room-*P* as well as at 8.08 GPa. It is worth pointing out that the intrinsic deformation of the tetrahedron in the structure of wardite is not due to the presence of P-O-H groups against P-O bonds, as occurs in other phosphates: all the hydroxyl groups of the wardite structure are bonded to the Al-octahedra.

As expected, Na- and Al-polyhedra also experience a compression of their bond distances in response to the applied pressure. For the two Al-octahedra, the differences in length of the Al-O bonds range between ~0.003 Å and ~0.04 Å, for a ΔP = 8.08 GPa, those of the Na-polyhedra between ~0.007 Å and ~0.07 Å. Overall, a pronouncedly different compression is usually expected among tetrahedra, octahedra and larger polyhedra coexisting in a given structure, as the tetrahedra are usually stiffer [27]. In this case, the compression of the P-tetrahedron (represented by its bulk modulus, Table S4) is similar, in magnitude, to that observed for the Al-octahedra, and lower than that of the Na-polyhedron. However, our reference scenario is that of silicates, as principal rock-forming minerals and the most studied class at non-ambient conditions. It is likely that what was previously observed in silicates is not simplistically extendable to phosphates.

Supplementary Materials: The following are available online at http://www.mdpi.com/2075-163X/10/10/877/s1, Table S1: Details pertaining to the structure refinements of wardite as a function of pressure; Table S2: (First *part*) Fractional atomic coordinates and atomic displacement parameters (Å^2) of wardite as a function of pressure (* data collected in decompression), (*Second part*) Selected bond distances (Å) at different pressure (* in decompression); Table S3: Evolution of the polyhedral volumes (in Å^3) with pressure in wardite. Average uncertainties on the volume values pertaining to the Na-polyhedron, Al-octahedra and P-tetrahedron are estimated to be ~0.3 Å^3, ~0.1 Å^3 and ~0.01 Å^3, respectively (on the basis of the largest and smallest volume values generated by the uncertainties of the bond distances); Table S4: Refined compressional parameters pertaining to the P-, Al- and Na-polyhedra in wardite, based on isothermal II -BM Equation of State fits (* fixed parameter).

Author Contributions: G.D.G. and D.C. conceived and designed the study, produced and managed the article structure; A.G. provided the sample, its mineralogical description and performed the electron microprobe analysis; G.D.G., P.L. and N.R. performed the SC-XRD characterization of the mineral sample in home lab at the Univ. Milan, whereas D.C. and M.H. collected the in-situ high-pressure data at ESRF; G.D.G., D.C. and P.L. discussed the results based on the experimental findings at high pressure. All authors have read and agreed to the published version of the manuscript.

Funding: G.D.G. and P.L. acknowledge the support from the Italian Ministry of Education (MIUR) through the project: "PRIN2017—Mineral reactivity, a key to understand large-scale processes" (2017L83S77).

Acknowledgments: ESRF is thanked for the allocation of beam time. Three competent reviewers are thanked for their suggestions aimed to improve the quality of the manuscript.

Conflicts of Interest: The authors declare no conflict of interest.

References

1. Davison, J.M. Wardite: A new hydrous basic phosphate of alumina. *Am. J. Sci.* **1896**, *2*, 154–155. [CrossRef]
2. Kampf, A.R.; Adams, P.M.; Housley, R.M.; Rossman, G.R. Fluorowardite, $NaAl_3(PO_4)_2(OH)_2F_2{\cdot}2H_2O$, the fluorine analog of wardite from the Silver Coin mine, Valmy, Nevada. *Am. Mineral.* **2014**, *99*, 804–810. [CrossRef]
3. Fanfani, L.; Nunzi, A.; Zanazzi, P. The crystal structure of wardite. *Mineral. Mag.* **1970**, *37*, 598–605. [CrossRef]
4. Gatta, G.D.; Guastoni, A.; Fabelo, O.; Fernandez-Diaz, M.T. A single-crystal neutron diffraction study of wardite, $NaAl_3(PO_4)_2(OH)_4{\cdot}2H_2O$. *Phys. Chem. Miner.* **2019**, *46*, 427–435. [CrossRef]
5. Breitinger, D.K.; Belz, H.H.; Hajba, L.; Komlósi, V.; Mink, J.; Brehm, G.; Colognesi, D.; Parker, S.F.; Schwab, R.G. Combined vibrational spectra of natural wardite. *J. Mol. Struct.* **2004**, *706*, 95–99. [CrossRef]
6. Frost, R.L.; Erickson, K.L. Near-infrared spectroscopic study of selected hydrated hydroxylated phosphates. *Spectrochim. Acta-Part A Mol. Biomol. Spectrosc.* **2005**, *61*, 45–50. [CrossRef]
7. Frost, R.L.; Xi, Y. A vibrational spectroscopic study of the phosphate mineral Wardite $NaAl_3(PO_4)_2(OH)_4{\cdot}2H_2O$. *Spectrochim. Acta Part A Mol. Biomol. Spectrosc.* **2012**, *93*, 155–163. [CrossRef]
8. Robertson, B.T. Occurrence of epigenetic phosphate minerals in a phosphatic iron formation, Yukon Territory. *Can. Mineral.* **1982**, *20*, 177–187.
9. Robinson, G.W.; Van Velthuizen, J.; Ansell, H.G.; Sturman, B.D. Mineralogy of the Rapid Creek and Big Fish River area, Yukon Territory. *Mineral. Rec.* **1992**, *23*, 1–47.
10. Mao, H.K.; Xu, J.; Bell, P.M. Calibration of the ruby pressure gauge to 800 kbar under quasi-hydrostatic conditions. *J. Geophys. Res.* **1986**, *91*, 4673. [CrossRef]
11. Angel, R.J.; Bujak, M.; Zhao, J.; Gatta, G.D.; Jacobsen, S.D. Effective hydrostatic limits of pressure media for high-pressure crystallographic studies. *J. Appl. Crystallogr.* **2007**, *40*, 26–32. [CrossRef]
12. Merlini, M.; Hanfland, M. Single-crystal diffraction at megabar conditions by synchrotron radiation. *High Press. Res.* **2013**, *33*, 511–522. [CrossRef]
13. *Rigaku Oxford Diffraction CrysAlisPro Software System, version 1.171.38.46; Rigaku Corporation:* Oxford, UK, 2018.
14. Petrícek, V.; Dušek, M.; Palatinus, L. Crystallographic computing system JANA2006: General features. *Z. Kristallogr.* **2014**, *229*, 345–352.
15. Birch, F. Finite elastic strain of cubic crystals. *Phys. Rev.* **1947**, *71*, 809–824. [CrossRef]
16. Gonzalez-Platas, J.; Alvaro, M.; Nestola, F.; Angel, R. EosFit7-GUI: A new graphical user interface for equation of state calculations, analyses and teaching. *J. Appl. Crystallogr.* **2016**, *49*, 1377–1382. [CrossRef]
17. Angel, R.J. Equation of State. In *High-Temperature and High Pressure Crystal Chemistry*; Hazen, R.M., Downs, R.T., Eds.; Mineralogical Society of America: Chantilly, VA, USA, 2000; pp. 35–59.

18. Angel, R.J.; Allan, D.R.; Miletich, R.; Finger, L.W. The use of quartz as an internal pressure standard in high-pressure crystallography. *J. Appl. Crystallogr.* **1997**, *30*, 461–466. [CrossRef]
19. Benusa, M.D.; Angel, R.J.; Ross, N.L. Compression of albite, $NaAlSi_3O_8$. *Am. Mineral.* **2005**, *90*, 1115–1120. [CrossRef]
20. Gatta, G.D.; Rotiroti, N.; Pavese, A.; Lotti, P.; Curetti, N. Structural evolution of a 3*T* phengite mica up to 10 GPa: An in-situ single-crystal X-ray diffraction study. *Z. Kristallogr.* **2009**, *224*, 302–310. [CrossRef]
21. Gatta, G.D.; Merlini, M.; Rotiroti, N.; Curetti, N.; Pavese, A. On the crystal chemistry and elastic behavior of a phlogopite 3*T*. *Phys. Chem. Miner.* **2011**, *38*, 655–664. [CrossRef]
22. Nestola, F.; Gatta, G.D.; Boffa-Ballaran, T. The effect of Ca substitution on the elastic and structural behavior of orthoenstatite. *Am. Mineral.* **2006**, *91*, 809–815. [CrossRef]
23. Pamato, M.G.; Nestola, F.; Novella, D.; Smyth, J.R.; Pasqual, D.; Gatta, G.D.; Alvaro, M.; Secco, L. The high-pressure structural evolution of olivine along the forsterite–fayalite join. *Minerals* **2019**, *9*, 790. [CrossRef]
24. Gatta, G.D.; Nestola, F.; Boffa-Ballaran, T. Elastic behaviour and structural evolution of topaz at high pressure. *Phys. Chem. Miner.* **2006**, *33*, 235–242. [CrossRef]
25. Gatta, G.D.; Merlini, M.; Valdrè, G.; Liermann, H.P.; Nénert, G.; Rothkirch, A.; Kahlenberg, V.; Pavese, A. On the crystal structure and compressional behavior of talc: A mineral of interest in petrology and material science. *Phys. Chem. Miner.* **2013**, *40*, 145–156. [CrossRef]
26. Gatta, G.D.; Lotti, P.; Merlini, M.; Liermann, H.P.; Lausi, A.; Valdrè, G.; Pavese, A. Elastic behaviour and phase stability of pyrophyllite and talc at high pressure and temperature. *Phys. Chem. Miner.* **2015**, *42*, 309–318. [CrossRef]
27. Hazen, R.M.; Downs, R.T.; Prewitt, C. Principles of Comparative Crystal Chemistry. In *High-Temperature and High Pressure Crystal Chemistry*; Hazen, R.M., Downs, R.T., Eds.; Mineralogical Society of America: Chantilly, VA, USA, 2000; pp. 1–33.

© 2020 by the authors. Licensee MDPI, Basel, Switzerland. This article is an open access article distributed under the terms and conditions of the Creative Commons Attribution (CC BY) license (http://creativecommons.org/licenses/by/4.0/).